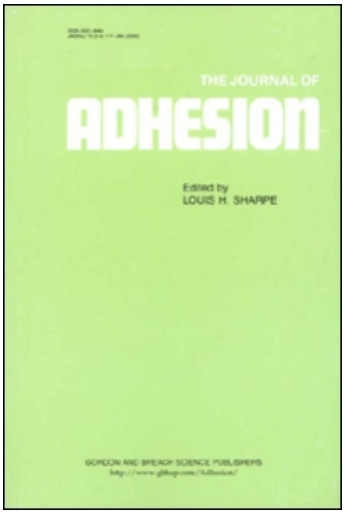

The Journal of Adhesion

Publication details, including instructions for authors and subscription information:
http://www.informaworld.com/smpp/title~content=t713453635

Nanoscale Indentation of Polymer Systems Using the Atomic Force Microscope

M. R. Vanlandingham[a]; S. H. McKnight[b]; G. R. Palmese[c]; J. R. Elings[d]; X. Huang[c]; T. A. Bogetti[b]; R. F. Eduljee[a]; J. W. Gillespie Jr.[a]

[a] Center for Composite Materials and Materials Science Program, University of Delaware, Newark, DE, USA [b] Army Research Laboratory, Weapons and Materials Research Directorate, Aberdeen Proving Ground, MD, USA [c] Center for Composite Materials, University of Delaware, Newark, DE, USA [d] Digital Instruments, Santa Barbara, CA, USA

To cite this Article Vanlandingham, M. R. , McKnight, S. H. , Palmese, G. R. , Elings, J. R. , Huang, X. , Bogetti, T. A. , Eduljee, R. F. and Gillespie Jr., J. W.(1997) 'Nanoscale Indentation of Polymer Systems Using the Atomic Force Microscope', The Journal of Adhesion, 64: 1, 31 — 59

To link to this Article: DOI: 10.1080/00218469708010531

URL: http://dx.doi.org/10.1080/00218469708010531

J. Adhesion, 1997, Vol. 64, pp. 31–59
Reprints available directly from the publisher
Photocopying permitted by license only

Nanoscale Indentation of Polymer Systems Using the Atomic Force Microscope*

M. R. VANLANDINGHAM[a], S. H. McKNIGHT[b], G. R. PALMESE[c], J. R. ELINGS[d], X. HUANG[c], T. A. BOGETTI[b], R. F. EDULJEE[a] and J. W. GILLESPIE, JR.[a,]**

[a]*Center for Composite Materials and Materials Science Program, University of Delaware, Newark, DE 19716, USA;*
[b]*Army Research Laboratory, Weapons and Materials Research Directorate, Aberdeen Proving Ground, MD 21005-5069, USA;*
[c]*Center for Composite Materials, University of Delaware, Newark, DE 19716, USA;*
[d]*Digital Instruments, Santa Barbara, CA 93103, USA*

(Received 28 October 1996; In final form 23 January 1997)

The use of the atomic force microscope (AFM) to measure surface forces has been developed to optimize its operation as a surface imaging tool. This capability can potentially be extended to evaluate nanoscale material response to indentation and would be ideal for the evaluation of multi-component polymer systems, such as adhesives and composites. In this paper, previous work related to the development of the AFM as a nanoindentation device is reviewed, and a technique is proposed which allows the AFM to be used to probe local stiffness changes in polymer systems. Cantilever probes with spring constants ranging from 0.4–150 N/m were used to investigate a number of polymer systems, including an elastomer, several polyurethane systems, thermally cured epoxies, a thermoplastic polymer-thermosetting polymer adhesive system, and a thermoplastic matrix composite.

Keywords: Atomic force microscope; force curves; indentation; elastic modulus; polymers; elastomer; polyurethane; epoxy; fiber-reinforced polymer composite; interphase regions

*One of a Collection of papers honoring Yuri S. Lipatov on the occasion of his 70th birthday, 10 July 1997.

**Corresponding author.

BACKGROUND

The use of polymers in multi-component and multi-phase systems, such as coatings, adhesives, composites, and electronic devices, requires sensitive, nanoscale property evaluation of polymer systems. In multi-component materials, nanoscale properties that control various aspects of material performance can be different from bulk properties. For example, the behavior of polymer composites is highly dependent on the interfacial strength between the fiber and matrix. However, interfacial strength is controlled by the matrix material adjacent to the fiber, referred to as the fiber-matrix interphase region. In several investigations, this interphase region has been shown to have properties significantly different from the bulk resin [1–6]. This observation is generally attributed to differences in local chemistry or microstructure. Experimental evidence of these property differences has been obtained using several different methods, each of which infer interphase properties indirectly from the test data [3–6].

The atomic force microscope (AFM) has the ability to measure differences in response directly. Traditionally, the AFM has been used as a nanoscale profilometer, measuring the topography of surfaces through direct contact between the surface and a probe tip mounted on the end of a cantilever microbeam. Development of the AFM's imaging capabilities has focused on the tip-surface interaction forces, leading to the utilization of the AFM as a surface force apparatus. In this mode (termed force mode), the AFM monitors the interaction forces, which can include van der Waals, magnetic, electrostatic, or capillary forces, as a function of the separation distance between the tip and the sample surface [7,8]. Generally, force mode is used for minimizing tip-sample forces during imaging [9], but this mode can potentially be used to configure the AFM to perform nanoindentation studies.

During AFM force mode, the probe tip is first lowered into contact with the sample, then indented into the surface, and finally lifted off the sample surface. Concurrently, a detection system measures the probe tip deflection. Our system is equipped with an optical detection system, in which a laser beam is reflected off the top of the probe and onto a segmented photodiode. Deflection of the probe tip, thus, produces a change in the photodiode voltage, V_t, which can be monitored as a function of the vertical displacement of the piezo actuator, Δz_p. In

Figure 1, a typical plot of V_t *versus* Δz_p, termed a "force curve," is shown. As the piezo moves toward the sample surface, the tip deflection voltage (V_t) remains constant until the probe tip makes contact with the surface (A to B in Fig. 1). Just before tip-sample contact is made, the probe tip can be pulled down to the surface by attractive forces, causing a small decrease in V_t (B to C in Fig. 1). Decreasing the piezo height further causes the cantilever to deflect in the opposite direction, resulting in an increased V_t signal (C to D in Fig. 1). During unloading (D to E in Fig. 1), the piezo retracts, reducing the cantilever deflection until the tip separates from the sample surface. Often, however, the tip adheres to the surface, causing a further decrease in V_t until the tip jumps out of contact (E to F in Fig. 1).

Colton and co-workers have investigated the force curves produced by the AFM when operating in force mode [7, 8, 10–12]. They have observed that these force curves contain information regarding the adhesive and nanomechanical properties of the material. The original study by Burnham and Colton [10] compared the force curves of gold, graphite, and an elastomer. Indentation was performed using a tungsten wire probe with a tip radius of 100–200 nm and an effective

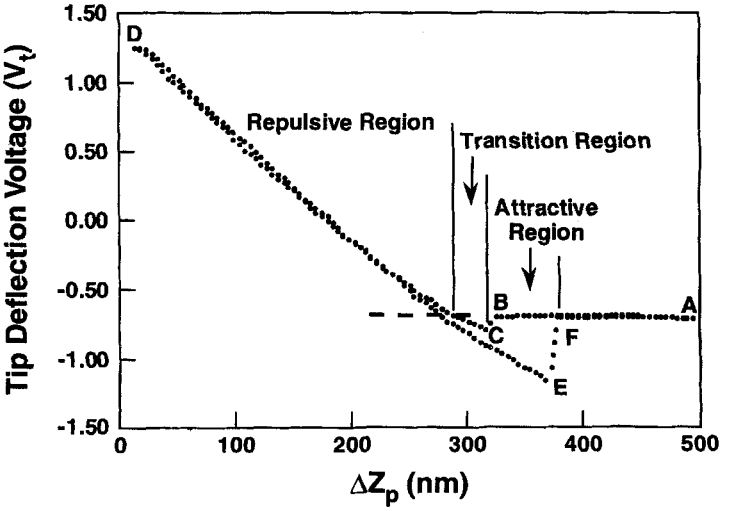

FIGURE 1 AFM force curve of a polyurethane sample ($E = 0.05$ GPa) measured using a 3 N/m probe.

spring constant measured to be 50 ± 10 N/m. Loads of around 1000 nN produced indentation displacements of 400 nm in the elastomer, and the load-unload curves were approximately linear and completely reversible. Indentation depths produced in graphite and gold were between 75 and 100 nm for loads of 4000 nN and 15000 nN, respectively. The loading curves were also observed to approach linearity for graphite and gold. Slight hysteresis was observed for the graphite upon unloading, but this could have been due to adhesion between the tip and the graphite surface. The gold foil sample showed no elastic component during unloading, however, behaving like an ideal plastic material. Using Sneddon's solution for a flat-ended cylindrical indenter [13] (discussed in the following section) with a contact radius of 100 nm and typical values of Poisson's ratio as inputs, modulus values were calculated from the unloading curves of graphite and the elastomer. The computed values fell within the wide modulus ranges quoted for each of the materials. Thus, the operation of the AFM as a nanoindentation device was demonstrated, but the accuracy of the computed modulus values was not assessed.

Several investigations [14–16], however, have revealed the importance of the contact stiffness,

$$S = \frac{\partial P}{\partial z} = \frac{2rE}{(1 - \nu^2)} \tag{1}$$

where P is the indentation load, z is the penetration depth, r is the contact radius, and E and ν are the sample's elastic modulus and Poisson's ratio, respectively. This parameter is the slope of the unloading curve and is valid for many indenter geometries. As will be discussed, the contact stiffness can be used to determine an appropriate spring constant for an AFM probe used to indent a material with a certain modulus. However, it does not produce an accurate measure of the relative stiffnesses of two materials. Hues *et al.* [8] have reported that initial slopes of unloading curves for several high modulus materials (*e.g.*, GaAs, mica, and silicon) indented with a diamond-tipped AFM probe did show reasonable correlation with elastic modulus. While the higher modulus materials did have steeper unloading slopes, the difference in slopes for two materials did not correspond directly to the difference in modulus. In general, the

relationship between indentation load and penetration depth will not be linear because of continuous changes in the contact area [17]. Thus, slope measurements will depend on the portion of the curve used to create a linear approximation [14] and will be a function of both the contact area and sample modulus.

To date, the majority of indentation studies have focused on metals and ceramics, which have elastic moduli that are several orders of magnitude greater than that of polymeric materials. Further, indentation apparatuses apply loads that create large indentations in polymer materials. The direct characterization of interphase regions in polymer systems, such as adhesives and composites, requires the ability to evaluate property changes over distances less than 1 μm. This type of nanoscale characterization is important in the evaluation of the long-term durability of polymer composites and adhesives. Many studies have shown that the combined effects of fatigue loading, changes in temperature, and exposure to moisture or solvents leads to degradation in properties and accumulation of damage [18]. Coatings and sizings can also break down over time due to similar service conditions [19]. These effects are often attributed to interfacial or interphasial degradation.

The imaging and indenting capabilities of the AFM make it an ideal tool for the evaluation of local properties of these complex polymer systems. While previous work does show promise, further development of the AFM's indentation capabilities, as well as a more complete understanding of the response of polymers to indentation, is required. In the following section, ideas developed in micro-indentation studies of metals and ceramics will be presented. These ideas will then be used to develop a more complete method for measuring nanomechanical properties of polymer samples with the AFM. This technique will include equations that allow the indentation response to be extracted from the force curve data. Finally, the application of this approach for probing homogeneous and multi-component polymer systems will be presented and discussed.

NANOSCALE MECHANICS

To develop relationships between indentation measurements and mechanical properties, several models have been used which describe

the contact between two elastic materials. In the Hertzian model, two elastic spheres of radii R_1 and R_2 make contact at a point. Setting $R_1 = \infty$ and $R_2 = R$ yields the geometry of a sphere of radius R indenting a flat surface. Upon loading, the surface deforms such that the radius of contact, r, increases with the amount of penetration, z, according to the Hertzian relation, $r = (R \cdot z)^{1/2}$ [7–12]. Removal of the load causes the contact area to decrease back to the initial point contact.

Improvements to this model were made by Johnson, Kendall, and Roberts (JKR) [20] and by Derjaguin, Muller, and Toporov (DMT) [21]. The JKR theory accounts for the short-range attractive forces local to the region of contact which typically can increase the contact area, while the DMT theory accounts for long-range attractive forces which act outside the contact region. In general, both the short-range and long-range attractions will occur, which can be accounted for using semi-empirical modeling [7]. Also, a thermodynamic approach developed by Maugis and Barquins accounts for viscoelastic deformation in the materials being indented [9]. These theories allow for the characterization of the adhesive properties of a surface using low contact loads. At high loads, they reduce to the Hertzian model, because the contact behavior will be more Hertzian when the contact forces are large relative to the surface forces [7]. Thus, for nanoindentation studies using stiff indenters and samples, local surface forces can generally be neglected, and the nanoscale mechanical response of the sample can be modeled using Hertzian mechanics.

The Hertzian model, however, does not account for effects due to geometry and inelastic deformation that can be important to the indentation process. In fact, in most indentation analyses, the Hertz theory is replaced by an analysis of the indentation of an elastic half-space generally attributed to Sneddon [13, 22]. Sneddon developed relationships between indentation depth, z, and load, P, for several different indenter geometries, all of which can be represented in the form

$$P = \frac{\xi E}{(1 - \nu^2)} z^m \tag{2}$$

where ξ is a constant which depends on the geometry of contact, E and ν are the sample's elastic modulus and Poisson's ratio, respectively,

and m is a power law exponent determined from a curve fit of P as a function of z. For behavior characteristic of a flat cylindrical punch, $m = 1$; for behavior characteristic of a paraboloid of revolution, $m = 1.5$; and for behavior characteristic of a cone, $m = 2$. Note that Sneddon's solution for a paraboloid of revolution gives identical results to the Hertz theory when the parameter, $2k$, in Sneddon's analysis [13] is set equal to the radius, R, of the Hertzian sphere.

The non-linearity of indentation unloading curves is due to the change in contact radius, r, with penetration depth, z. Eq. (2) can be restated to allow for the determination of the contact geometry in the following form:

$$P = \frac{\xi' E}{(1 - \nu^2)} z \tag{3}$$

where

$$\xi' = \xi z^{m-1} \tag{3a}$$

Using results due to Sneddon, the parameter ξ' can be related directly to the contact radius by

$$\xi' = \frac{2r}{m} \tag{4}$$

Thus, for a material of known modulus and Poisson's ratio, the indentation geometry can be evaluated from the P-z unloading curve, which is assumed to contain pure elastic recovery.

The exponent, m, is thus a parameter which is characteristic of the geometry of indentation. As argued by Bolshakov, Oliver, and Pharr [23], however, the geometry of indentation does not necessarily correspond to the indenter geometry. This conclusion came about as a result of finite element modeling [23] that was used to explain the non-linear unloading curves of nanoindentation experiments. Many indentation studies [14,24–29] have observed that, for a wide range of materials, indentation unloading curves are non-linear with power law exponents, m, ranging from 1.2 to 1.5. The indenters normally used in these studies are sharp-tip cones or pyramids, but the m values do not

correspond with that for a conical indenter. This effect is due to plastic deformation in the vicinity of the indenter tip during the loading process. This plastic deformation removes the elastic singularity at the tip and creates a plastic hardness impression that, along with the indenter geometry, determines the effective shape of indentation during unloading. This effective indenter shape can be modeled as a body of revolution by an equation of the form [23]

$$Z = BR^n \tag{5}$$

where B is a constant and R is the radial distance from the axis of symmetry of the indenter, as shown schematically in Figure 2. For this type of indenter shape, Sneddon's analysis yields a solution which again can be represented by Eq. (2). From this solution, the exponents, m and n, are shown to be related by

$$m = 1 + \frac{1}{n} \tag{6}$$

such that n values ranging from 2 to 5 yield the observed m range of 1.2 to 1.5. The geometric parameters, ξ and ξ', in Eqs. (2), (3), and (4) are also shown to be directly related to n. This analysis correctly predicts that the contact area will change continuously during indentation. Thus, the power law parameters generated from a curve fit of the unloading data define the geometry of the indentation process, given a known value of E and a reasonable estimate of ν [25].

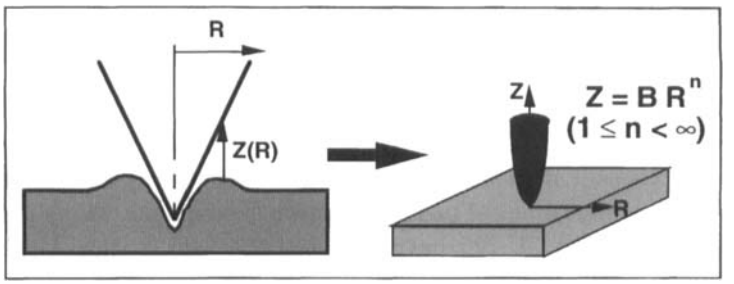

FIGURE 2 The effective shape of the indenter is derived from the difference between the plastic impression after unloading and the indenter shape [15].

Without an independent assessment of the contact area, absolute modulus values cannot be determined. This restriction arises because the proportionality factor, α, in the power law equation ($P = \alpha z^m$ (abbreviated version of Equation (2))) contains both the geometric parameter, ξ, and the sample modulus, E. If the same force range is used to indent two materials, if the resulting power law exponents, m, are the same, and if equivalent Poisson's ratios for the two materials are assumed, then the indentation response of material 1 to that of material 2 can be related as follows:

$$\frac{\alpha_1}{\alpha_2} = \frac{\xi_1 E_1}{\xi_2 E_2} = \left[\frac{(\Delta z_i)_2}{(\Delta z_i)_1}\right]^m \tag{7}$$

Combining Equations (3a) and (4), substituting the result for ξ_1 and ξ_2, and combining like terms, it can be shown that

$$\frac{(\Delta z_i)_2}{(\Delta z_i)_1} = \frac{r_1 E_1}{r_2 E_2} \tag{8}$$

Therefore, the elastically recovered indentation displacements, Δz_i, for the two materials could be used to calculate the ratio of material moduli if the contact radii could be related or are assumed to be equal. For multi-component systems, in general, both r and E are unknowns and only one independent equation exists that relates them. In our studies, indenting soft polymer samples of known moduli with AFM probe tips, using maximum forces on the order of 100–6000 nN, has produced contact radius values that are larger than values predicted using either a geometric approximation or the Hertzian model ($r = (R \cdot z)^{1/2}$). (Here, we approximate the tip as a conical indenter with a cone angle of 18° and a finite tip radius $R = 10$ nm). This result is shown in Figure 3 for responses of two polyurethane samples which were characterized by $m \approx 1.5$ (*i.e.*, Hertzian-like behavior). The Hertzian and geometric models will generally give a lower bound of contact area because they do not account for the effects of plastic deformation or local attractive forces. Using either one of these models to estimate r would lead to substantial error in the calculated modulus value.

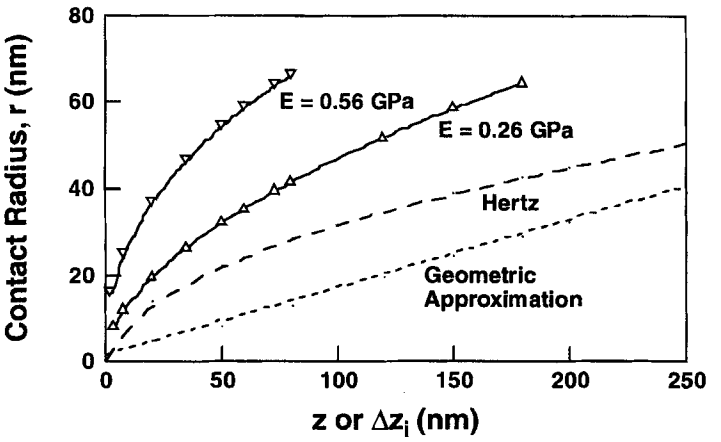

FIGURE 3 Contact radius, r (nm), as a function of indentation depth, z or Δz_i (nm), based on three different models - a geometric model, the Hertzian model, and a power law model fitted to experimental data. Data were calculated from the indentation response of two polyurethanes with moduli of 0.56 and 0.26 GPa, respectively, indented with a 50 N/m probe with a maximum force of approximately 5000 nN.

EXPERIMENTAL

An atomic force microscope was used as both a surface imaging tool and an indentation device to evaluate the nanoscale response of polymer samples. For the experimental investigations, a Digital Instruments D3000 scanning probe microscope was used to produce force curves from the interaction of four types of cantilever probes and a number of polymer samples. The effective spring constants of the four types of probes were estimated to be 0.4–0.6 N/m, 1–5 N/m, 20–100 N/m, and 150 ± 15 N/m. Herein, these probe types will be referred to as flexible (0.4–0.6 N/m), medium (1–5 N/m), stiff (20–100 N/m), and diamond-tipped (150 ± 15 N/m).

The flexible probes were 120 μm in length and were made of silicon nitride in a V-frame configuration, each leg having a width of 40 μm and a thickness of 0.4–0.6 μm. The tips were located at the intersection of the legs (*i.e.*, at the tip of the V), having heights of 3 μm and radii of approximately 20–40 nm. The medium and stiff probes were 225 μm and 125 μm, respectively, in length and were made of silicon in a single-beam configuration with widths of 30–40 μm and thicknesses of 2–5μm. The tips of these single-beam silicon probes were

located near the end of the microbeams, having heights of 10–15 μm and radii of 5–10 nm. Probe and tip dimensions for the flexible, medium, and stiff probes are as quoted by the manufacturer. Width and thickness variations along the cantilevers and between probes of the same type do exist and are responsible for the large uncertainty in the spring constant values. This uncertainty further hinders the calculation of absolute modulus values from indentation data.

A diamond-tipped stainless steel cantilever was used for investigations of multi-component systems. The stainless steel cantilever had a width of 100 μm, a thickness of 12.7 μm, and a length of 275 μm. The diamond tip had a height of approximately 100–120 μm and a tip radius estimated to be 10–20 nm. The effective spring constant for this probe was measured using a technique developed at Digital Instruments, which utilizes a digital microbalance to measure applied forces as a function of the deflection of the cantilever probe.

The polymer samples consisted of crosslinked polydimethylsiloxane (PDMS) (see Reference 30 for details), several polyurethanes, and several epoxy samples. The polyurethanes were processed from polyester polyol/TDI-based diisocyanate prepolymers. By varying the functional groups between the cyanate groups, these prepolymers were developed to have different chain flexibilities. The resulting polymer samples exhibited similar mechanical behavior but with different elastic moduli. Epoxy samples were processed with different ratios of epoxy to amine curing agent, again yielding samples with different elastic modulus values [2,3]. The epoxy was EPON 828®, manufactured by Shell Corp., and the curing agent was PACM 20 amine, manufactured by Air Products, Inc. Multi-component systems consisted of a thermoplastic polyimide composite reinforced with graphite fibers (IM7/K3B) manufactured and fabricated by the DuPont Company [31], and an adhesive system created by allowing the previously described epoxy-amine system to diffuse into a fully formed thermoplastic polymer, polysulfone, during cure at 60°C. Details of the latter system are found elsewhere [32,33].

The elastic moduli of polymer samples used in this study were determined independently using dynamic mechanical analysis (DMA) and ranged from 0.5 MPa for the PDMS up to 3.5 GPa for the unreinforced K3B matrix resin. DMA was performed using a three-point bend loading fixture and a frequency of 1 Hz. Each of the sam-

ples (except for PDMS) was prepared for study with the AFM by sectioning with a band saw, mounting in an epoxy potting compound, grinding with 320 and 600 grit sand paper, and polishing to a 0.05 μm finish using a variety of diamond pastes and alumina particle slurries.

In order to provide a calibration reference, a sapphire sample (E = 470 GPa [34]) was used as an "infinitely stiff" material for the determination of C_θ from Eq. (13). After obtaining a minimum of 10 force curves for the sapphire sample, a minimum of 10 individual force curves was obtained under the same operating conditions for each polymer sample of interest. The rate of loading was such that one load-unload cycle was complete in approximately 1 to 5 seconds. To ensure that the calibration parameter, C_θ, did not change during testing, a second set of force curves was obtained for the sapphire sample after indentation testing was completed. Each force curve was then analyzed according to the methodology outlined in the following subsection.

AFM Indentation Technique

To extract the nanoscale mechanical response of the material from the contact portion of the force curve, the tip-sample interaction is modeled as two springs in series, as shown in Figure 4. After contact is made between the probe tip and the sample surface, piezo displacement re-

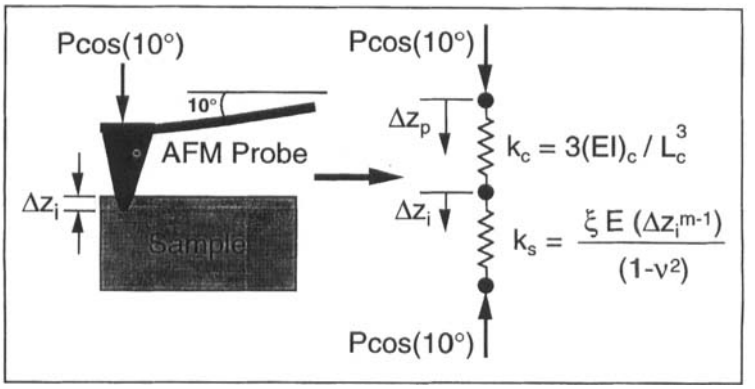

FIGURE 4 Schematic and spring model of tip-sample contact during AFM force mode operation.

sults in both probe tip deflection and sample indentation, the amounts of which depend on the relative stiffnesses of the sample and the cantilever probe [34, 35]. The relationship between the displacement of the piezoelectric actuator (Δz_p), the displacement due to tip deflection (Δz_t), and the indentation displacement (Δz_i) is simply

$$\Delta z_i = \Delta z_p - \Delta z_t \cos(10°) \tag{9}$$

where the cos(10°) term corrects for the angle of the probe to the horizontal, as shown in Figure 4. The probe force, P, can be calculated directly from the probe tip displacement by

$$P = k_c \Delta z_t \tag{10}$$

where k_c is the spring constant of the cantilever probe. The resolution of the calculated forces is generally on the order of 1 to 50 nN, depending on cantilever stiffness, because the noise on the tip displacement detector limits depth resolution to 0.1 nm [8]. To calculate the force applied to the sample, P is multiplied by cos(10°) to again account for the 10° angle of the probe.

For a sample which is infinitely stiff with respect to the probe, no indentation will occur and $\Delta z_p = \Delta z_t$. From simple beam theory and considering the 10° angle of the probe, the angle change of the cantilever at the tip ($\Delta\theta_t$) and the tip displacement (Δz_t) are related by

$$\Delta\theta_t = \frac{3\Delta z_t}{2L_c \cos(10°)} \tag{11}$$

where L_c is the length of the cantilever probe. This angle change is directly related to the change in photodiode voltage, V_t, by system conversion and calibration factors [34] which can be lumped into a constant, C_θ, such that

$$\Delta\theta_t = \frac{\Delta V_t}{C_\theta} \tag{12}$$

Combining Eqs. (11) and (12), the slope of the force curve, Σ, is shown to have an upper limit, Σ^*, given by

$$\Sigma^* = \frac{\Delta V_t}{\Delta z_p} = \frac{3C_\theta}{2L_c \cos(10°)} \tag{13}$$

For a sample that deforms due to the force applied by the probe, Σ will be reduced from Σ^* by a reduction factor, f (*i.e.*, $f = \Sigma/\Sigma^*$), such that larger values of f correspond to stiffer samples. Also, the amount of indentation, Δz_i, at different points along the force curve can be calculated using Eq. (9). The applied force, P, can also be calculated using Eq. (10) if k_c is known. The indentation displacement, Δz_i, is then related to the applied force, P, through the relation given in Eq. (2).

RESULTS AND DISCUSSION

Contact Stiffness *versus* Probe Spring Constant

Preliminary studies were performed to evaluate the potential of the AFM as an indentation device. Flexible, medium, and stiff probes were used to indent polymers with a range of modulus values. The rate of loading was such that one load-unload cycle was complete in approximately 1 second. Good correlation between the generated force curve data and the sample moduli was observed. The slope reduction factor, f, was observed to increase as the stiffness of the sample increased. For each cantilever probe with a spring constant less than 100 N/m, however, the f values approached one for polymers with moduli above a certain value [36, 37]. Similarly, the ratio of the maximum indentation displacement relative to a maximum probe tip displacement of 100 nm is sensitive to changes in modulus up to 0.5 and 0.05 GPa for the stiff and medium probes, respectively, as shown in Figure 5. For these lower stiffness probes, the applied force is insufficient to produce adequate deformation of the stiffer samples (such as the epoxy samples, for which $E = 2.0$–3.0 GPa). For a given tip displacement, a stiffer probe applies higher forces to the sample than does a probe of lower stiffness. Therefore, it can be used to evaluate higher modulus samples.

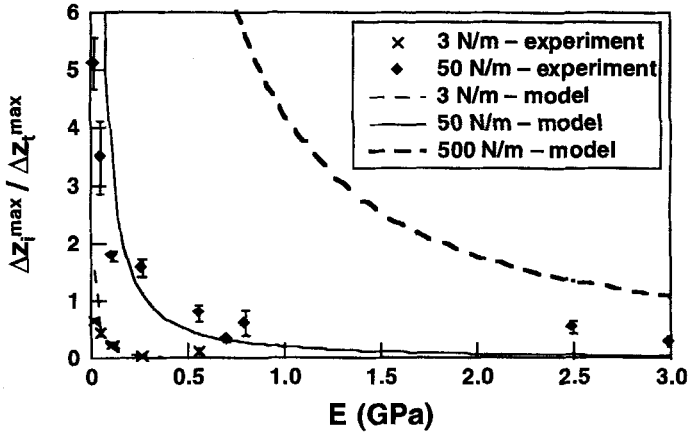

FIGURE 5 Ratio of maximum indentation displacement, Δz_i^{max}, to a maximum tip displacement, Δz_t^{max}, of 100 nm plotted as a function of sample modulus, E.

Also shown in Figure 5 are curves generated using the spring model shown schematically in Figure 4 and outlined in Eqs. (2), (9), and (10). Input values typical of experimentally measured responses were used to calculate values of Δz_i corresponding to $\Delta z_t = 100$ nm for silicon probes with spring constants of 3, 50, and 500 N/m. The model results correspond well to the experimental data. Due to limitations of the optical detection system, the maximum tip displacement that can be accurately applied is between 100 and 200 nm (depending on the dimensions and properties of the silicon cantilever), thus limiting the applied force for a given cantilever probe. Therefore, extremely stiff probes ($k_c \approx 500$ N/m) will be required to probe modulus changes in polymers commonly used in engineering applications.

Both the experimental results and the results of the spring model indicated that cantilever selection should be based on the expected range of moduli. As mentioned previously, the contact stiffness, defined in Eq. (1), can be used to determine an appropriate probe spring constant. For example, a polymer with $E = 0.3$ GPa and $\nu = 0.4$ which is indented with an etched silicon probe producing contact radii ranging from 10–100 nm will have a contact stiffness during indentation of $S = 7$–70 N/m. From experimental observation, stiff probes ($k_c = 20$–100 N/m) are generally sufficient to indent this material while the medium and flexible probes produce little to no sample

deformation. For indentation of a polymer with $E = 3$ GPa under similar conditions, $S = 70$–700 N/m; thus a much stiffer probe would be required to produce measurable deformation.

Lateral Motion Effects

As mentioned previously, the load-indentation data extracted from the force curve can be characterized by a power law expression (Eq. (2)). For the probe-polymer combinations used in our studies, the values of the power law exponent, m, generally fell into a narrow range, typically between 1.1 and 1.6. The overall range of m observed was between 0.9 and 1.9, indicating that the geometry of the indentation produced could vary widely for polymer samples indented with sharp-tipped probes. For individual samples, however, the range of m values typically varied by ± 0.15 about a mean value. This variation could be due in part to two separate system effects. First, because the vertical motion of the piezo actuator is not completely uncoupled from the lateral motions, small lateral translations (on the order of nanometers) can occur during testing. Second, the cantilever probe is mounted at a 10° angle from the horizontal plane, as shown in Figure 4, and can slide laterally on the sample surface while applying force to the sample [38]. In any case, the variation in m results in a variation in the proportionality factor, α. Assuming a specific geometry (*e.g.*, Hertzian, for which $m = 1.5$), as is common in previous studies [8, 10, 12, 24–27, 29, 34, 35], would lead to substantial scatter in either calculated contact radius values (with E known) or estimated modulus values (with r approximated).

To reduce the lateral motion effects inherent in our AFM system, new software was developed by Digital Instruments [38] to provide a compensating lateral motion. This compensation attempts to counteract the moment acting on the cantilever due to the reaction forces at the surface, as shown in Figure 6. As the cantilever bends, the deflection due to the surface normal force produces a rotation of the tip which, in turn, causes the contact point of the tip to translate laterally. However, local deformation and topography generally will restrict this lateral motion; thus a lateral surface force is generated that bends the cantilever in the direction opposing the bend due to the normal force. (Note that the mechanics of indentation for traditional apparatuses do not include lateral forces.) On a force curve plot, this effect will

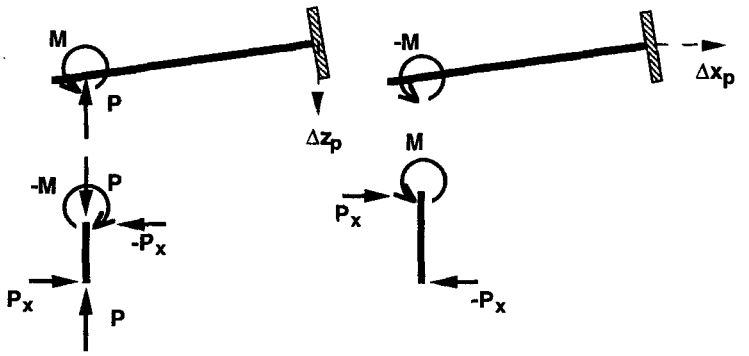

(a)

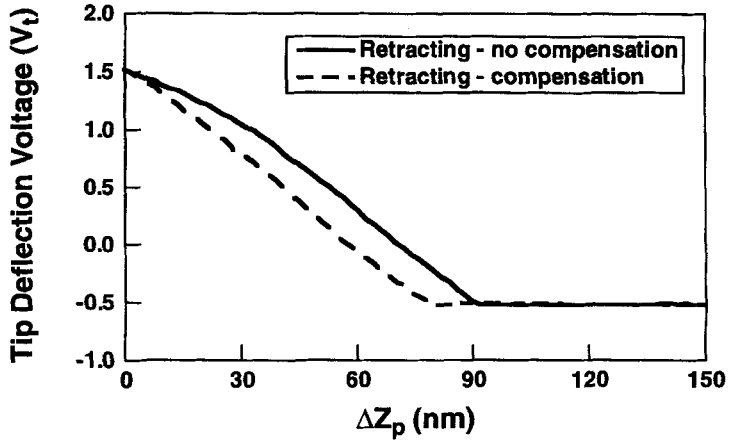

(b)

FIGURE 6 (a) Free-body diagrams of cantilever and probe tip for z and x displacements of the piezo actuator; and (b) a comparison of the retracting portion of two force curves, taken for a diamond-tip probe on a sapphire surface under the same operating conditions, except one was taken using lateral motion compensation, while the other was taken without compensation.

result in a decrease in the slope with increasing tip deflection (see Fig. 6b). Therefore, a lateral translation of the probe that is proportional to the vertical translation during indentation testing would counteract this effect, such that the measured deflection of the probe tip is due only to the surface normal force. Further, because the angle of beam deflection is on the order of 0.1°, a linear proportionality

between the lateral compensating translation and the vertical displacement seems appropriate. In Table I, results of analytical and finite element models calculating the ratio of lateral to vertical motion for several different probe geometries are presented. These values were used to refine our technique for the experimental results that follow. Also, in the studies to follow, attempts were made to position the start and end points of the probe tip just above the sample surface and as close to the surface as possible. This procedure reduces the total motion of the piezo so that piezo hysteresis and coupled translation effects are limited.

Homogeneous Polymer Systems

The majority of results to date are for the indentation of homogeneous polymer systems. Initial studies provided insight into the importance of the probe's spring constant relative to the sample stiffness, and have helped in the development and refinement of this technique. For these purposes, low modulus ($E < 1$ GPa) polyurethane and elastomeric systems were quite useful.

Polyurethanes

Five polyurethane samples were processed from polyester polyol/ TDI-based diisocyanate prepolymers with different chain flexibilities. From the results of DMA, the room-temperature modulus values of the five polyurethanes were 0.02, 0.05, 0.11, 0.26, and 0.56 GPa. The indentation responses of these systems were similar. Large amounts of elastic deformation, as measured in the unloading response, were observed, and the hysteresis between the load and unload curves depended on the magnitude of the maximum load. Typical load-

TABLE I Calculations of the ratio of lateral (x-) motion to vertical (z-) motion of the piezo actuator using an analytical model and a finite element model for several AFM probe geometries

Probe Type	*Probe Length* / *Tip Height*	***Analytical Model*** *x-motion* / *z-motion*	***Finite Element Model*** *x-motion* / *z-motion*
stiff	8.2	0.35	0.34
diamond-tipped	2.5	0.78	0.80

indentation curves for the 0.26 GPa and 0.56 GPa samples, measured using a stiff probe, a maximum load of 5000 nN, and a rate of 1 load-unload cycle per 5 seconds, are shown in Figure 7. The calculated m values are quite similar, indicating similar unloading geometries (see Fig. 3), but the total amount of indentation, as well as the amounts of elastic deformation and load-unload hysteresis, is larger for the lower modulus material. This observation indicates that for these materials, as the penetration depth increases, the deformation zone increases such that both elastic and inelastic deformations increase. The higher modulus material is more resistant to penetration, because the contact stiffness, S, is larger than for the lower modulus polymer.

PDMS

A model study was performed using a flexible and a medium AFM probe to indent a PDMS sample with a bulk modulus measured to be 0.5 MPa using DMA. Several other experimental observations of this material [30] indicated that the surface layer exposed to air during processing developed a higher crosslink density and, thus, a higher modulus than the interior. Therefore, an attempt was made to investigate the relative stiffness of the surface and interior regions of the

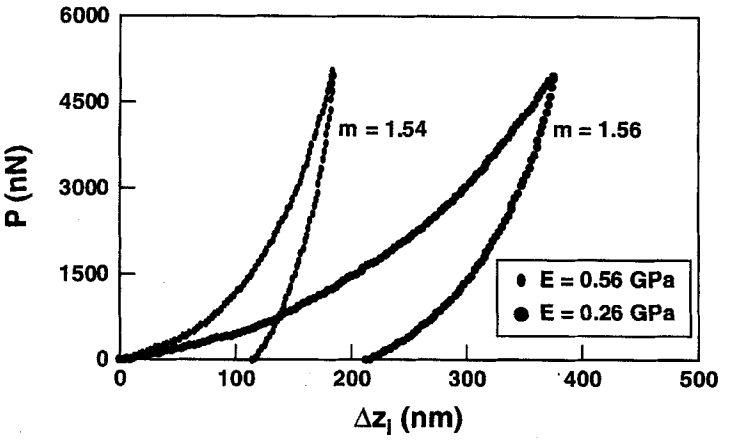

FIGURE 7 Comparison of load-indentation curves with similar m values for the 0.56 and 0.26 GPa polyurethane samples. Both samples were indented using a 50 N/m probe to apply a maximum force of approximately 5000 nN.

PDMS elastomer using the AFM. The interior was exposed simply by slicing off a substantial portion of the surface. No other surface preparation was needed for this material.

The indentation response of the elastomer was shown to be completely reversible, as no load-unload hysteresis was measured using penetration depths from 30 to 500 nm. Significantly higher penetration depths were observed in the interior material than in the surface layers for each maximum applied force level, as shown in Figure 8. The largest difference was noticed at lower load levels where, for a maximum load of around 30–40 nN, the ratio of indentation displacement of the interior to that of the surface was 2.4. As the maximum load was increased to approximately 150 nN, this ratio decreased to 1.1. In these studies, the load-unload cycle time remained at 5 seconds, such that the actual loading rate increased with increasing load levels. However, this relatively small change in loading rate is not expected to cause such a large change in indentation behavior, particularly for an elastomeric material which, at room temperature, is well above its glass transition temperature. More likely, this result was due to an increasing contribution to the response of the surface from the core material as the penetration distance increased. Unfortunately, the thickness of the higher-modulus surface layer was not determined from independent tests.

Another interesting result was observed using the flexible silicon nitride probe, which had an estimated tip radius of 20–40 nm. This probe was used at the lowest applied load range of 30–40 nN, resulting in indentation depths of around 25 nm for the surface and 60 nm for the interior. The calculated m values fell within a small range around $m = 1$ (see Fig. 8b), indicating that the contact radius did not change significantly during indentation. This result could be due to the combination of two effects. First, because the applied loads were so small, adhesive forces between the tip and the sample might have been significant, creating a large contact area at the onset of tip-sample contact. Then during penetration, the maximum depths obtained were on the order of twice the blunted tip radius such that the contact area would have remained reasonably constant during indentation. If so, then the indentation displacement ratio of 2.4 between the interior and surface is approximately equal to the ratio of the surface modulus to the interior modulus using Eq. (8). Results from

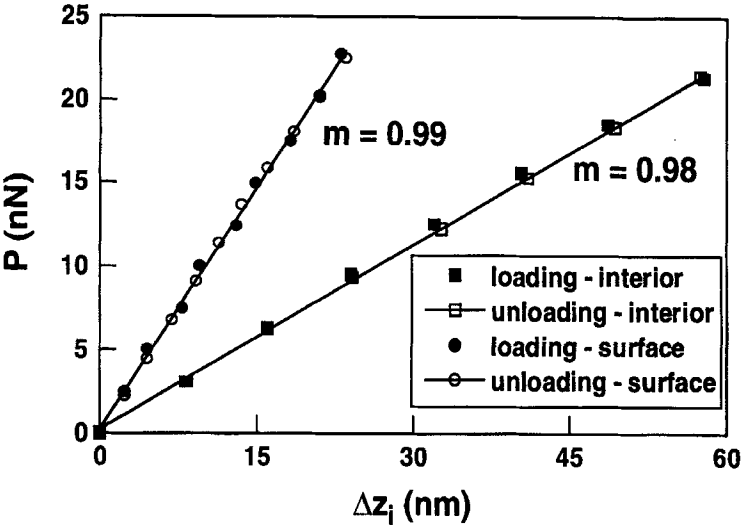

(a)

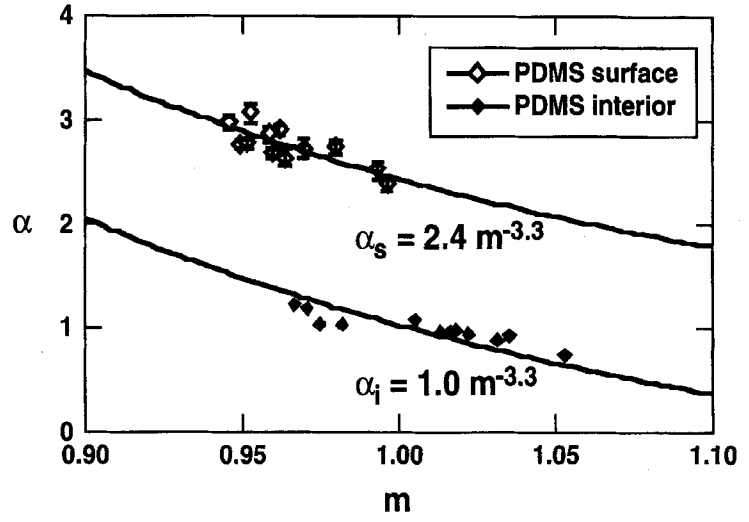

(b)

FIGURE 8 Indentation response of a PDMS sample. A large difference in elastic response between the surface and interior was observed; (a) linear, reversible load-unload curves for which the penetration into the interior is much larger than that for the surface layer; and (b) power law front factor, α, as a function of the power law exponent, m, which yields a stiffness ratio of 2.4 between the surface and interior.

JKR adhesion experiments with this PDMS material [30] indicated that the surface modulus was approximately a factor of two above the bulk value measured using DMA. Thus, these two sets of results are in good agreement.

Multi-Component Systems

The ability of the AFM to indent polymers using loads ranging from 20 to 10000 nN and creating indentation displacements ranging from 30 to 500 nm has been demonstrated. Studies of a diffuse polymer-polymer interphase and a fiber-matrix interphase were performed to determine the sensitivity of this technique for evaluating local property variations which can be important in the performance of these material systems. To indent these higher modulus ($E > 2$ GPa) systems, the diamond-tipped indenter was used. This indenter offers a higher spring constant than the silicon probes, and the cantilever is significantly longer, allowing a larger amount of detectable tip displacement. Because of these attributes, much larger maximum forces can be applied.

Polymer-Polymer Adhesive System

Indentation was performed as part of a study in which the properties of a bond between epoxy and polysulfone were evaluated. This bond was created by placing an uncured mixture of an epoxy-amine system (described previously) between two slabs of a fully-formed thermoplastic polymer (polysulfone), which had been previously bonded to aluminum adherends. This system was then exposed to a temperature of 60°C for 2 hours to allow the epoxy-amine mixture to diffuse into the thermoplastic and cure. The extent of the diffusion of the epoxy into the polysulfone was estimated using several methods to be between 2 and 3 μm [32,33]. Indentations were made over a total distance of approximately 5 μm, stepping laterally with increments of 200 to 300 nm. The diamond-tipped probe was used to apply a maximum indentation force of 4500 nN with a loading rate such that one load-unload cycle was complete in approximately 1 second. Also, the surface was imaged after indentation was performed to evaluate changes in the sizes of the plastic impressions.

A variety of responses was measured across the polymer-polymer bond. The bulk epoxy, in general, exhibited slightly larger amounts of

elastic recovery and less inelastic deformation than the bulk polysulfone. This observation is most likely due to differences in mechanical behavior. Although the modulus values are similar (2.3 GPa for the epoxy *versus* 2.5 GPa for the polysulfone), thermosetting polymers, such as the epoxy, are generally much more brittle, exhibiting much lower levels of plasticity than thermoplastic polymers due to the nature of crosslinking *versus* chain entanglement. The interphase region produced responses similar to the bulk epoxy in some cases, responses similar to bulk polysulfone in some cases, and responses different from either of the bulk materials in other cases.

The elastic response of the bulk materials, characterized by power law front factors (α) for various power law exponents (m), is shown in Figure 9. A curve fit of α as a function of m, while perhaps not physically meaningful, does show two different trends for the two bulk materials. The responses from the interphase region tend to lie between these two curves. Differences in the sizes of the plastic impressions, which were often larger in the interphase region than in the bulk materials, were used to estimate the width of the interphase at approximately 3 μm. This estimation agrees with estimations of the interphase size from energy-dispersive X-ray spectroscopy, electron microscopy, and AFM imaging [33].

Although lateral motion compensation was used in this study, the power law exponent, m, still showed variations over the surface of the bulk samples. This observation could be due to local variations in properties and/or microstructure or to error in the technique. Studies of microstructural effects on the indentation response and a more thorough error analysis of the technique are underway.

Polymer Composite

Indents were made near a graphite fiber in a 60% volume fraction thermoplastic polyimide composite (IM7/K3B) [31]. Maximum applied loads were approximately 3000 nN, the rate of loading was such that one load-unload cycle was complete in approximately 1 second, and indents were made radially outward from the fiber using step sizes of less than 100 nm. For indents nearest the fiber, deformation was significantly restricted by the presence of the fiber because the fiber modulus is much greater than the matrix modulus. Using the indentation mechanics presented previously, an apparent stiffening of the

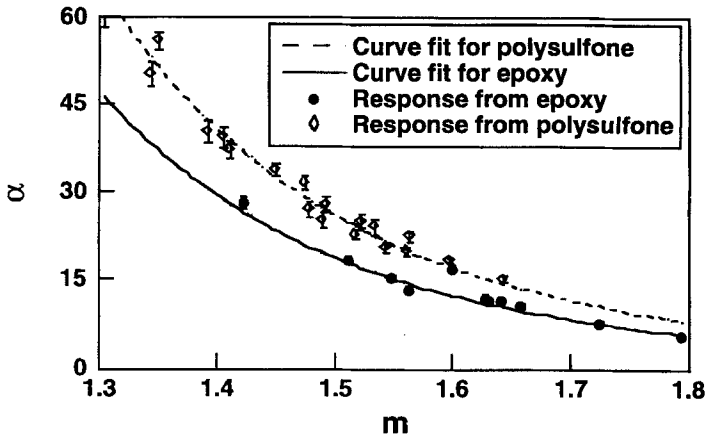

(a)

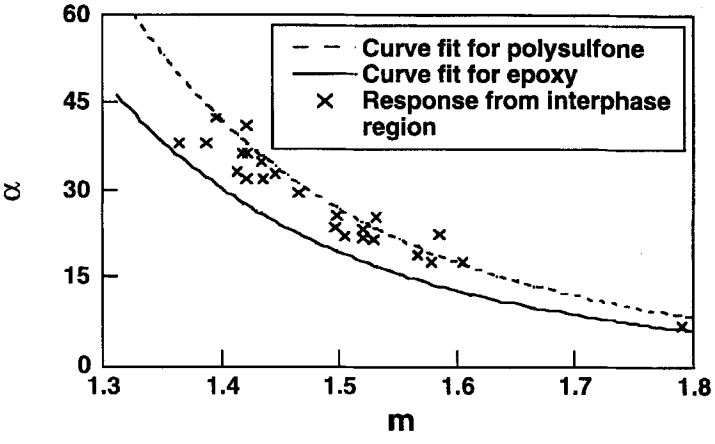

(b)

FIGURE 9 Plot of the power law front factor, α, as a function of the power law exponent, m, for the epoxy-polysulfone system; (a) two different dependencies exist for the bulk material; and (b) the response of the interphase material lies between the responses of the bulk polymers.

matrix material results [6]. This effect was modeled using finite element analysis. A two-dimensional axisymmetric model was shown to produce results similar to a three-dimensional model in much less computation time. Results from this model are shown in Figure 10

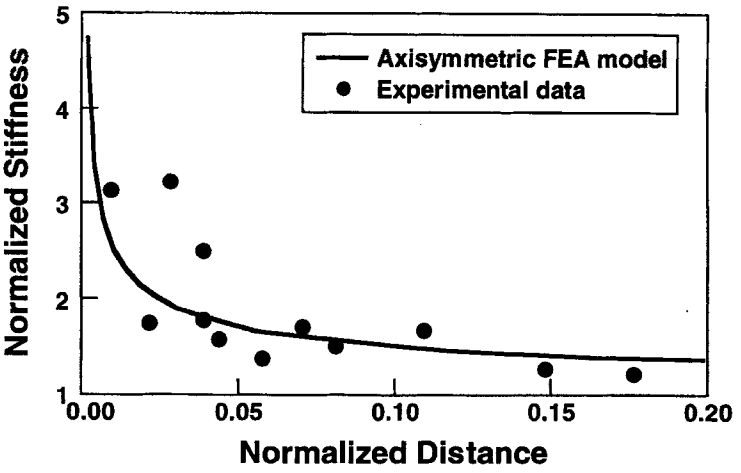

FIGURE 10 Plot showing the stiffening effect of the fiber to local deformation of the matrix. Experimental data are shown along with the predictions of a finite element model. Stiffness is normalized with respect to the bulk behavior, and the normalized distance is the distance from the fiber divided by the fiber diameter.

using constitutive properties representative of the IM7/K3B system [31]. Also shown in Figure 10 are the experimental results. For the model, normalized stiffness is defined as the force divided by the indentation displacement normalized to that in the bulk polymer (*i.e.*, away from the fiber). For the experimental data, a normalized stiffness (similar to contact stiffness) is calculated using Eq. (8), where material 2 is the bulk polymer and material 1 is the material indented at a certain distance from the fiber. The normalized distance is then just the distance from the fiber divided by the fiber diameter, which is 5 μm for the IM7 fiber. In the case where displacement continuity is maintained across the fiber-matrix interface, a significant increase in the apparent matrix modulus is expected as the fiber surface is approached. Thus, the results of the model correspond to experimentally-measured responses.

CONCLUSIONS

The development of a technique that utilizes the atomic force microscope (AFM) as a nanoindentation device has been presented. This

technique allows for the indentation response to be extracted from AFM force curve data. Unloading curves were characterized by a power law relation between load and indentation displacement that was developed from elasticity theory. Power law exponents varied over a small range of values for a single sample, but were observed to vary from $m = 1$ to $m = 2$ for a large number of probe-polymer combinations. This range of power law exponents corresponds to changes in the effective geometry controlling elastic recovery during unloading. Results to date have been used to determine a range of probe spring constants necessary to indent a material with a certain elastic modulus. The contact stiffness was shown to be a useful parameter for estimating the resistance of a polymer to indentation by a probe with a known spring constant. Also, refinements to the technique allow for the compensation of lateral forces and motions that create sources of error.

Indentation tests were performed on several homogeneous polymer systems. A set of polyurethanes with modulus values ranging from 0.02 to 0.56 GPa responded in a similar manner to indentation loads. Both elastic and inelastic deformation increased with penetration depth of the indenter. Indentation of an elastomeric material, PDMS ($E = 0.5$ MPa), with flexible AFM probes produced large elastic deformation at low applied loads with virtually no inelastic deformation. A skin-core effect was observed, in which the surface layer of the sample deformed less than the interior material. This effect was due to a higher degree of crosslinking of the surface material during processing. A factor of 2.4 was estimated for the ratio of the surface modulus to the interior modulus.

Two multi-component polymer systems were studied using the AFM indentation technique. Indentation across a polymer-polymer adhesion system produced a variety of responses. The response of the interphase material was different from the responses of either the bulk epoxy or the bulk polysulfone. These differences were used to estimate the width of the interphase at approximately 3 μm. Indents were also made near a graphite fiber in a 60% volume fraction thermoplastic matrix composite. Deformation was significantly restricted for indents nearest the fiber. This effect leads to an apparent stiffening of the matrix material which was measured experimentally and modeled using finite element analysis. The step size across interphase regions is

limited by the size of the plastic impressions and the geometry of the interphase. Step sizes much less than 100 nm can be achieved with a lateral resolution of 0.1 nm. Thus, the capability of the AFM to probe local material response to indentation has been demonstrated.

FUTURE WORK

Future work will focus on the use of diamond-tipped stainless steel and super-stiff silicon cantilevers to probe relatively high modulus ($E > 2.0$ GPa) homogeneous and multi-component polymer systems. In particular, the relative amounts of elastic, plastic, and viscoelastic deformation will be studied to understand better the differences in indentation behavior between polymers with similar mechanical properties. Also, the contribution of tip-sample adhesion to the load-unload hysteresis at low levels of applied load needs to be explored. Once these effects are understood, changes in indentation behavior between different polymer samples or across surfaces of multi-component systems will be more meaningful.

While this technique shows promise, several factors must be addressed to extend the capabilities of the AFM as a probe of local property variations. One such area to be studied will be the effect of time-dependent behavior on the measured response. In this work, a constant load-unload cycle time was used. However, changing several independent force mode parameters allows the loading rate to be changed by orders of magnitude. Thus, future studies will include a more detailed characterization of the relative amounts of time-dependent behavior involved. To date, significant time-dependent deformation has been observed only at loading rates much lower than those used in this work.

Other important factors that will influence the success of this technique include the relationship between local microstructure and indentation response. Also, the lack of simple methods to measure spring constants of AFM probes hinders the ability to calculate applied forces and, thus, to calculate accurate modulus values. Several fairly complex methods exist [39,40], while a simpler method using a Nanoindenter to deflect the probes directly [41] is limited by the instrument's load and depth resolution capabilities. A technique used

at Digital Instruments, which utilizes a digital microbalance to measure applied forces, shows the most promise for the simple, accurate measurement of probe spring constants. Lastly, a thorough error analysis of this technique needs to be completed. With a firm understanding of these effects, a more quantitative evaluation of nanoscale property variations important in complex material systems can be made.

Acknowledgements

The authors gratefully acknowledge the support of the U. S. Army Research Laboratory (ARL) under the Composite Materials Research Collaborative Program (CMRCP), ARL agreement number DAAL01-96-2-0048. Also, the authors at the University of Delaware appreciate the close interactions with scientists and engineers at Digital Instruments which continue to play a large role in the development of this technique.

References

[1] Lipatov, Y. S. and Babich, V. F., *Mechanics of Composite Materials* **23**, 15–21 (1987).
[2] Palmese, G. R. and McCullough, R. L., *J. Adhesion* **44**, 29–49 (1994).
[3] Skourlis, T. P. and McCullough, R. L., *Composites Science and Technology* **49**, 363–368 (1993).
[4] Sottos, N. R. and McCullough, R. L., *Flight-Vehicle Materials, Structures and Dynamics: Assessment and Future Directions* **2**, 328–350 (1994).
[5] Madhukar, M. S. and Drzal, L. T., *J. Composite Materials* **25**, 958–991 (1991).
[6] Williams, J. G., Donnellan, M. E., James, M. R. and Morris, W. L., *Materials Sci. and Eng.* **A126**, 305–312 (1990).
[7] Burnham, N. A., Colton, R. J. and Pollock, H. M., *J. Vacuum Sci. Technol. A* **9**, 2548–2556 (1991).
[8] Hues, S. M., Colton, R. J., Meyer, E. and Guntherodt, H.-J., *MRS Bulletin* **18**, 41–49 (1993).
[9] Aime, J. P., Elkaakour, Z., Odin, C., Bouhacina, T., Michel, D., Curely, J. and Dautant, A., *J. Appl. Phys.* **76**, 754–762 (1994).
[10] Burnham, N. A. and Colton, R. J., *J. Vacuum Sci. Technol. A* **7**, 2906–2913 (1989).
[11] Burnham, N. A., Colton, R. J. and Pollock, H. M., *Nanotechnology* **4**, 64–80 (1993).
[12] Hues, S. M., Draper, C. F. and Colton, R. J., *J. Vacuum Sci. Technol. B* **12**, 2211–2214 (1994).
[13] Sneddon, I. N., *Internat. J. Eng. Sci.* **3**, 47–57 (1965).
[14] Oliver, W. C. and Pharr, G. M. J., *Materials Res.* **7**, 1564–1583 (1992).
[15] Jarvis, S. P., Weihs, T. P., Oral, A. and Pethica, J. B., *Materials Research Society Symposium Proc.* **308**, 127–132 (1993).
[16] Pethica, J. B. and Oliver, W. C., *Physica Scripta* **T19**, 61–66 (1987).
[17] King, R. B., *Intern. J. Solids and Struct.* **23**, 1657–1664 (1987).

[18] Weitsman, Y., *Intern. J. Solids and Struct.* **23**, 1003–1025 (1987).
[19] Plueddemann, E. P., *Silace Coupling Agents*, 2nd ed. (Plenum Press, New York, 1992).
[20] Johnson, K. L., Kendall, K. and Roberts, A. D., *Proc. Roy. Soc. A* **324**, 301–309 (1971).
[21] Derjaguin, B. V., Muller, V. M. and Toporov, Y. P., *J. Colloid Interface Sci.* **53**, 314–320 (1975).
[22] Johnson, K. L., *Contact Mechanics* (Cambridge University Press, London, 1985).
[23] Bolshakov, A., Oliver, W. C. and Pharr, G. M., *Materials Research Society Symposium Proc.* **308**, 201–208 (1993).
[24] Oliver, W. C., Hutchings, R. and Pethica, J. B., *Microindentation Techniques in Materials Science and Engineering*, **ASTM STP 889**, Blau, P. J.and Lawn, B. R., Eds. (American Society for Testing and Materials, Philadelphia, 1986), pp. 90–108.
[25] Doerner, M. F. and Nix, W. D., *J. Materials Res.* **1**, 601–609 (1986).
[26] Loubet, J. L., Georges, J. M., Marchesini, O. and Meille, G., *J. Tribology* **106**, 43–48 (1984).
[27] Pethica, J. B., Hutchings, R. and Oliver, W. C., *Philosophical Magazine A* **48**, 593–606 (1983).
[28] Pharr, G. M., Oliver, W. C. and Brotzen, F. R., *J. Materials Res.* **7**, 613–617 (1992).
[29] Stillwell, N. A. and Tabor, D., *Proc. Phys. Soc. London* **78**, 169–178 (1961).
[30] Chin, P, "Characterization of Polymer-Solid Adhesion By the JKR Theory," Ph.D. Dissertation, University of Delaware, Newark, DE (1996).
[31] Wedgewood, A. R., *Proc. Nineteenth International SAMPE Tech. Conf.* pp. 420–434, 1987.
[32] Immordino, K. M., McKnight, S. H. and Gillespie, J. W., Jr., *Proc. Fifty-Fourth Tech. Conf. Society of Plastics Engineers (ANTEC'96)* **402**, 1214–1218 (1996).
[33] Immordino, K. M., "Characterization of the Epoxy-Polysulfone Interphase for Bonding Thermoplastic Composites," Masters Thesis, University of Delaware, Newark, DE (1996).
[34] Maivald, P., Butt, H. J., Gould, S. A. C., Prater, C. B., Drake, B., Gurley, J. A., Elings, V. B. and Hansma, P. K., *Nanotechnology* **2**, 103–106 (1991).
[35] Weisenhorn, A. L., Khorsandi, M., Kansas, S., Gotzos, V. and Butt, H.-J., *Nanotechnology* **4**, 106–113 (1993).
[36] VanLandingham, M. R., McKnight, S. H., Palmese, G. R., Eduljee, R. F., Gillespie, J. W., Jr. and McCullough, R. L., *J. Materials Sci. Lett.* submitted (1996).
[37] VanLandingham, M. R., McKnight, S. H., Palmese, G. R., Eduljee, R. F., Gillespie, J. W., Jr. and McCullough, R. L., *Proc. Eleventh Tech. Conf. American Soc. for Composites* to be published (1996).
[38] Elings, J. R., Support Note No. 225, Digital Instruments, Santa Barbara, CA, 1996.
[39] Cleveland, J. P., Manne, S., Bocok, D. and Hansma, P. K., *Rev. Sci. Insts.* **64**, 403–405 (1993).
[40] Hutter, J. L. and Bechhoefer, J., *Rev. Sci. Insts.* **64**, 1868–1873 (1993).
[41] Weihs, T. P., Hong, S., Bravman, J. C. and Nix, W. D., *J. Materials Res.* **3**, 931–942 (1988).